Engineering Structures 201 (2019) 109775

Contents lists available at ScienceDirect

Engineering Structures

journal homepage: www.elsevier.com/locate/engstruct

Vibration control for torsionally irregular buildings by integrated control system

Osman Akyürek[a], Nakin Suksawang[b,*], Tiauw Hiong Go[c]

[a] Department of Civil Engineering, Nevsehir Haci Bektasi Veli University, Nevsehir, Turkey
[b] Department of Mechanical and Civil Engineering, Florida Institute of Technology, 150 W University Blvd, Melbourne, FL 32901, United States
[c] Department of Aerospace, Physics and Space Science, Florida Institute of Technology, 150 W University Blvd, Melbourne, FL 32901, United States

ARTICLE INFO

Keywords:
Torsional irregularity
RC building
Code provision
SAC project
Benchmark building
ICS

ABSTRACT

Torsion irregularity increases the risk of building failure during a strong dynamic excitation that is generated by earthquakes or wind gusts. To enhance the safety and performance of torsional irregular buildings, a newly developed Integrated Control System (ICS) is proposed in this research. The new control approach was applied to a two-way eccentric Benchmark 9-story steel building, constructed for the SAC steel project in California, where each floor is represented by two translational and one rotational degree of freedom. The performance and effectiveness of the ICS were examined and compared with a Tuned Mass Dampers (TMDs) approach by subjecting the building to real earthquake excitations of N-S and E-W components of El Centro in 1940, Loma Prieta in 1989, and Kocaeli, Turkey in 1999. Results showed that the ICS was effectively mitigating the lateral and coupling vibrations by the new design configuration and arrangement for both tuning and detuning cases. The ICS is also more robust in restricting the inter-story drift ratio as compared with TMDs.

1. Introduction

The development of advanced technologies and structural material in the 21st century have led to taller and more flexible buildings using lighter materials. This trend makes buildings less damping and becoming more susceptible to dynamic loadings such as severe wind gusts and earthquakes, especially for those having complex shapes where torsion becomes an issue. Torsional irregularity exists when the center of mass (CM) that the total mass of a body is assumed concentrated and stiffness (CS)—which is the distribution of the lateral load-resisting members within a story, including braced frames, moment frames, and walls—are not coincident. In such condition, the structures will tend to twist as well as deflect horizontally under an earthquake excitation as illustrated in Fig. 1 [1,2].

Damage assessments in the field investigation of few past earthquakes have frequently revealed that buildings with irregular plan configuration have more severe damage due to excessive torsional responses and stress concentration than corresponding regular buildings [3]. The plan configuration irregularities introduce major challenges in the seismic design of buildings. Therefore, many researchers have studied on torsional irregularity and its definition to take into consideration of this irregularity in the seismic design provisions. Özhendekci and Polat, 2008 [4] have introduced parameter Q, which is a ratio of the effective modal masses, and it can be used to define the torsional irregularity of buildings. Özmen et al., 2014 have been studied in determining the conditions for excessive torsional irregularity and then to discuss the validity of code provisions. They proposed a new provisional definition for torsional irregularity coefficient based on floor rotations [5].

The traditional method to protect the buildings against torsional sensitivity is by adding the bracing systems into structure frames [6–8]. It is a simple and effective way to enhance the safety and performance for torsionally irregular buildings (TIBs) under bidirectional earthquake excitations because it does not only increase the lateral and torsional load capacity, but also eliminate the lack of coincidence between CM and CS. The system can be a k- or x-bracing frame system for steel [9–11] or masonry infill wall for reinforced concrete structure [12].

Many innovative smart control systems have been developed so far to protect the structures effectively against severe earthquake and wind loads. The most commonly and intensively used passive control system, thanks to its simplicity and cost, is a tuned mass damper (TMD), which adds external damping, stiffness, and mass to the main structure without using any external energy sources [13,14]. However, TMD has its drawbacks. It can be tuned only to the fundamental frequency of the structure so that it is effective only in the small range of frequency. It may have little or no effect on the other modes other than the one that

* Corresponding author.
E-mail addresses: oakyurek2015@my.fit.edu (O. Akyürek), nsuksawang@fit.edu (N. Suksawang), yongki@alum.mit.edu (T.H. Go).

https://doi.org/10.1016/j.engstruct.2019.109775
Received 16 April 2019; Received in revised form 29 August 2019; Accepted 7 October 2019
Available online 16 October 2019

Nomenclature

$x(t)$	lateral displacement in the x-direction with respect to time
$y(t)$	lateral displacement in the y-direction with respect to time
$\theta(t)$	angular motion with respect to time
$\dot{x}(t)$	lateral velocity in the x-direction with respect to time
$\dot{y}(t)$	lateral velocity in the y-direction with respect to time
$\dot{\theta}(t)$	angular velocity with respect to time
e_x	eccentiricity in the x-direction
e_y	eccentiricity in the y-direction
e	absolute eccentiricty between CM and CS
α	eccentricity angle
h	height of the floor
B, D	plan dimensions the x- and y-direction
x_s	lateral displacement of the center of stiffness (CS) in the x-direction
y_s	lateral displacement of the center of stiffness (CS) in the y-direction
θ_s	angular displacement of the center of stiffness (CS)
x_m	lateral displacement of the center of mass (CM) in the x-direction
y_m	lateral displacement of the center of mass (CM) in the y-direction
θ_m	angular displacement of the center of mass (CM)
CM	center of mass
CS	center of stiffness
$CRot$	center of rotation
r_x, r_y	radius of gyration of the structure in the x- and y-directions
r	absolute radius of gyration
L_1, L_2	initial length of the first and second TMD in ICS configuration
$r_1(t)$, $r_2(t)$	diagonal response of the first and second TMD in ICS configuration
$\theta_1(t)$, $\theta_2(t)$	angular displacement of the first and second TMD in ICS configuration
T	kinetic energy
V	potential energy
R	Rayleigh's dissipation function
F	external force for each dynamic component of the
M	mass matrix
I_m	polar mass
m_{d1}, m_{d2}	mass of the first and second TMD in ICS configuration
K_x, K_y, K_θ	stiffness of the main structure in the x- and y-translational and θ-directions
M_{st}, C_{st}, K_{st}	nxn matrix of mass, damping, and stiffness of the structure
$\delta(t)$, $\dot{\delta}(t)$, $\ddot{\delta}(t)$	n dimensional displacement velocity and acceleration vector
$\ddot{x}_g$, $\ddot{y}_g$	input ground motions in the × and y-direction
Γ	modification vector of the earthquake excitation
$Z(t)$	$(2nx1)$ state vector
A	$(2nx2n)$ system matrix
B	$(2nx2)$ input matrix
C_r , D_r	$(nx2n)$ and $(nx2)$ output matrix and direct transmission matrix
μ_1, μ_2	mass ratio of the first and second TMD in ICS configuration
ξ_{d1}, ξ_{d2}	damping ratio of the first and second TMD in ICS configuration
k_{d1}, k_{d2}	stiffness of the first and second TMD in ICS configuration
c_{d1}, c_{d2}	damping of the first and second TMD in ICS configuration
$L_1 + r_1^{max}$, $L_2 + r_2^{max}$	total length of torsional pendulum parts of ICS
μ_{qu}	mass ratio of the ICS in the torsional direction
ξ	structural damping ratio
w_x, w_y, w_θ	natural circular frequency in in the x- and y-translational and θ-directions
k	equivalent stiffness for a simple connected frame and a moment resisting frame
I_c,I_b	respectively moment of inertia for selected beams and columns
E	elasticity of the material
J_1	maximum floor displacement
J_2	maximum floor drift
J_3	maximum floor acceleration
$\lvert\delta_i(t)\rvert$	absolute displacement of the controlled system at the ith floor
δ^{max}	maximum absolute displacement of the uncontrolled system at any floor
$\lvert d_i(t)\rvert$	inter-story drift of the floor above ground level
h_i	height of the ith floor
d_n^{max}	maximum absolute inter-story ratio at any floor
$\lvert\ddot{\delta}_i(t)\rvert$	absolute displacement of the controlled system at the ith floor
$\ddot{\delta}^{max}$	maximum absolute acceleration of the uncontrolled system at any floor
E_{ir}	relative input energy
E_{kr}	relative kinetic energy
E_d	damping energy
E_a	strain energy

is used for its tuning process in the scenario of a dynamic load. Therefore, Xu and Igusa, 1992 [15] first proposed to use a multi-tuned mass damper (MTMD) to enhance its effectiveness.

Additionally, several studies [16–23] have increased the system stability at a wide range of frequencies of the MTMD system by tuning it to different natural frequencies. In addition to TMD systems, many other innovative control techniques have been successfully applied to improve the structural safety for TIBs such as base isolation systems (BIS) [24], hybrid base isolation systems (HBIS) [25,26] and circular tuned liquid column dampers (CTLCD) [27]. Base isolation systems with different bearing materials which have highly nonlinear behavior have been adequately studied by many researchers so far [28]. The engineering community accepts these techniques as practical ways of controlling lateral and torsional response.

The performance of TMD, which is optimally designed for only unidirectional loading case, is significantly reduced due to torsion and found to be less effective for the torsionally coupled system in comparison to the uncoupled system. This is because torsionally coupled buildings have at least two lateral and one torsional mode of vibration dominating the structural responses. At least two TMDs are, thus, required to control both lateral and torsional response of the system. The arrangements of those TMDs can be independently applied in both orthogonal directions [29,30] or can be eccentrically connected to one mass [31] or can be placed in such a way that is controlling for the torsional mode of vibration effectively [32]. Therefore, the different alternative arrangements of the TMD are studied by many researchers to increase the performance and safety of the torsionally coupled buildings.

According to the current researches, significant attention has currently been paid on the torsional response control by one or a set of TMDs. The improvements are overall achieved using several traditional TMDs [33–36] or the optimization of the TMDs placed in either the same or two orthogonal directions. However, only a few researchers concentrate on the innovative approach about the new configuration

[37,38] and the form of TMD or MTMDs according to the structural and ground motion characteristics. In this research, a new Integrated Control System (ICS), which utilizes a new configuration of TMDs, is proposed. The new control design approach was applied to the two-way eccentric Benchmark 9-story steel building, constructed for the SAC project in California, where each floor was represented by two translational and one rotational degree of freedom. ICS has the following contributions; (*i*) it employs multi tuned mass dampers (MTMD) and other components such as a torsional damper, springs, rigid rod and global bearing system to work together as a single control system, which is useful in controlling torsional response in addition to the lateral responses, (*ii*) each mass can be used for both a TMD and pendulum system thanks to the rigid rod, so this can make the system more feasible, because it is not always possible to add multiple masses, which might be too much to be carried by, on the top floor of the main structures, (*iii*) the torsional response reduction can be substantially obtained, and the tuning design of the ICS is flexible because it depends upon the initial length of the TMD, the damper and spring parameters, the mass ratio and the location of the ICS, so the ICS is highly capable of enhancing the control capacity of the structure conveniently in multi-directions. The performance and effectiveness of the ICS were examined and compared with the Tuned Mass Dampers (TMDs) approach under the data from the real earthquake excitations of N-S and E-W components of El Centro in 1940, Loma Prieta in 1989, and Kocaeli, Turkey in 1999. The results indicated that the ICS could effectively mitigate the coupling and orthogonal vibrations, by the new design configuration and arrangement, under bidirectional loading cases.

2. Integrated control system (ICS)

A traditional tuned mass damper (TMD) is only operative in the direction placed and only operative in the frequency of the main structure tuned. Hence, it has only little effects in controlling the torsional response. In order to alleviate this limitation in the research, the ICS was proposed, which is not only effective in horizontal directions but also effective in the torsional direction. A three-dimensional illustration of the proposed ICS and its implementation is shown in Fig. 2.

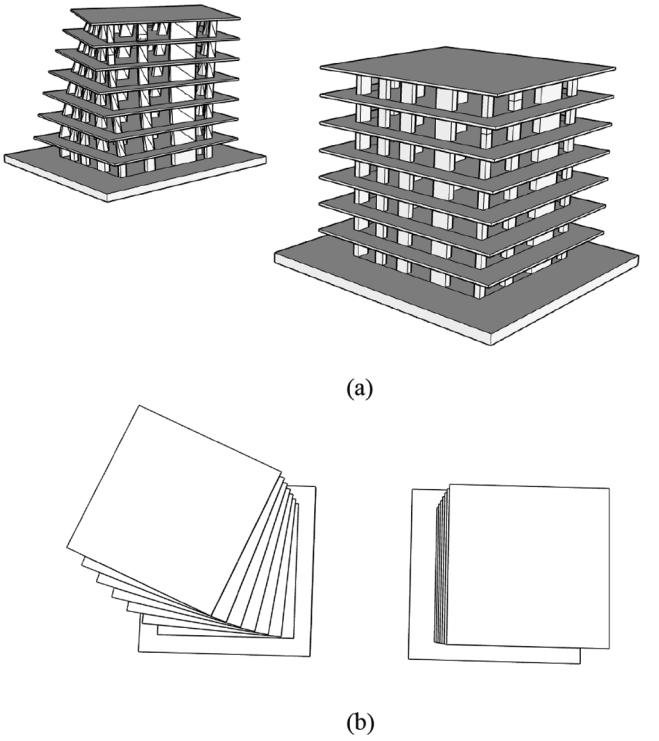

Fig. 1. Three-dimensional civil structure representation and its torsional mode: (a) elevation view; (b) plan view.

The ICS consists of two TMDs along two horizontal axes of the structure. It employs appropriate linear spring, linear damper, and additional mass into the main structure to ensure TMDs can dissipate undesirable energy appropriately. Additionally, the TMDs are placed in each orthogonal direction, and they can move in an orthogonal or torsional direction. The tuning design of the ICS is flexible ion with the help of the rigid rod and global bearing systems (tires). The motion of the TMDs in torsional direction is restricted by the torsional damper located at the CM and torsional springs, where one end is attached to the rigid rod (not the mass of the TMDs), and another end is fixed to the floor. The rigid rod has a negligible small mass as compared to the other components, and thus it is assumed as massless in the analysis. Each mass in the ICS composition can be used by the TMD as well as being used as a mass of the pendulum system with the aid of the rigid rod. In such a condition, it can make the system more feasible because it is not always possible to add multiple masses. They can be very heavy to be carried on the top floor of the main structure. The structural design configuration of the ICS is shown in Fig. 2.

The masses of the TMDs move back and forth from the equilibrium position in the two horizontal directions as well as rotational direction when the structure is subjected to earthquake excitations. They produce the inertia forces due to relative displacements and the rotational inertia force with the help of the rigid rod. While the linear damper and spring of the TMDs produce damping force and restoring force, the torsional damper and the torsional spring provide suitable rotational damping and restoring torques into the system. Hence, the structural responses can be effectively controlled in the two orthogonal directions as well as in the rotational direction by the ICS.

3. Structural dynamics and mathematical modelling

3.1. The dynamic equation for one-story two-way eccentric model building with the proposed ICS

A torsionally irregular one-story shear building, which is under the effects of bidirectional earthquake excitation in horizontal directions, has three degrees of freedom (DOF) for each story including lateral displacement in two directions and rotation at the center of the mass. In this structure, $x(t)$ represents lateral displacement in the x-direction, $y(t)$ is lateral displacement in the y-direction, $\theta(t)$ is the angular motion with respect to time.

The 3-D view of a torsionally coupled structure and the proposed control system can be seen in Fig. 3a and b. The center of stiffness and mass are represented with CS and CM, respectively. The distance between these centers is shown with e_x and e_y, and α is the eccentricity angle. It is assumed that the location of the center of mass is lumped at the center of each floor. B and D are the lengths of the structure in the x- and y-direction, respectively, and h is the height of the structure. The displacements and velocities of the center of stiffness and mass in translational directions and torsional direction can be mathematically expressed as follows:

The location of the CS is as follow

$$\begin{bmatrix} x_s \\ y_s \\ \theta_s \end{bmatrix} = \begin{bmatrix} x(t) \\ y(t) \\ \theta(t) \end{bmatrix}, \quad \begin{bmatrix} \dot{x}_s \\ \dot{y}_s \\ \dot{\theta}_s \end{bmatrix} = \begin{bmatrix} \dot{x}(t) \\ \dot{y}(t) \\ \dot{\theta}(t) \end{bmatrix} \tag{1}$$

The location of the CM with respect to the CS is

$$\begin{bmatrix} x_m \\ y_m \\ \theta_m \end{bmatrix} = \begin{bmatrix} x(t) - e_x.\ cos(\theta) \\ y(t) - e_y.\ \cos(\theta) \\ \theta(t) \end{bmatrix}, \quad \begin{bmatrix} \dot{x}_m \\ \dot{y}_m \\ \dot{\theta}_m \end{bmatrix} = \begin{bmatrix} \dot{x}(t) + e_x.\ \dot{\theta}(t)\cos(\theta) \\ \dot{y}(t) + e_y.\ \dot{\theta}(t)cos(\theta) \\ \dot{\theta}(t) \end{bmatrix} \tag{2}$$

One story building and the ICS applied in the x- and y-direction is

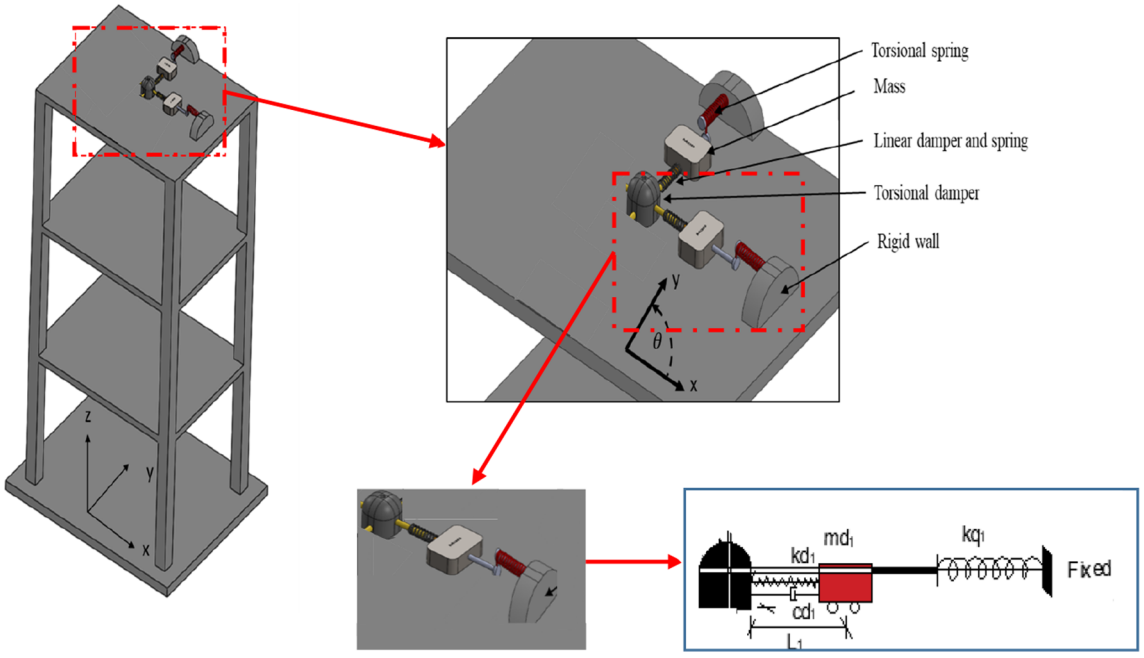

Fig. 2. 3-D illustration of the three-story civil structure and the proposed control system representation.

respectively simplified, and the Lagrangian energy method is used to derive the equation of motion. The kinetic and potential energies are, therefore, computed for each link in polar coordinate. In this model, each part of the ICS moves in between x- and y-direction like open-chain robotic arms as seen in Fig. 4, where CRot denotes the center of rotation, which is a point that does not move in rotation while the rest of the plane rotates around it. The distance between CRot and CM is defined as the radius of gyration (r). The position and velocity of the md1 and md2 are then given by

$$\begin{bmatrix} x_1 \\ y_1 \end{bmatrix} = \begin{bmatrix} \{L_1 + r_1(t)\}cos(\theta_1) \\ \{L_1 + r_1(t)\}sin(\theta_1) \end{bmatrix}, \quad \begin{bmatrix} x_2 \\ y_2 \end{bmatrix} = \begin{bmatrix} -\{L_2 + r_2(t)\}sin(\theta_2) \\ \{L_2 + r_2(t)\}cos(\theta_2) \end{bmatrix} \tag{3}$$

$$\begin{bmatrix} \dot{x}_1 \\ \dot{y}_1 \end{bmatrix} = \begin{bmatrix} cos(\theta_1) & -\{L_1 + r_1(t)\}sin(\theta_1) \\ sin(\theta_1) & \{L_1 + r_1(t)\}cos(\theta_1) \end{bmatrix} \begin{bmatrix} \dot{r}_1(t) \\ \dot{\theta}_1(t) \end{bmatrix} \tag{4}$$

$$\begin{bmatrix} \dot{x}_2 \\ \dot{y}_2 \end{bmatrix} = \begin{bmatrix} -sin(\theta_2) & -\{L_2 + r_2(t)\}cos(\theta_2) \\ cos(\theta_2) & -\{L_2 + r_2(t)\}sin(\theta_2) \end{bmatrix} \begin{bmatrix} \dot{r}_2(t) \\ \dot{\theta}_2(t) \end{bmatrix} \tag{5}$$

Lagrange energy method for each state variable where i is equal to m, 1 and 2, respectively, as follows:

$$\frac{d}{dt}\left(\frac{\partial T}{\partial \dot{x}_i, \partial \dot{y}_i, \partial \dot{\theta}_i}\right) - \left(\frac{\partial T}{\partial x_i, \partial y_i, \partial \theta_i}\right) + \left(\frac{\partial R}{\partial \dot{x}_i, \partial \dot{y}_i, \partial \dot{\theta}_i}\right) + \left(\frac{\partial V}{\partial x_i, \partial y_i, \partial \theta_i}\right) = F_{x_i, y_i, \theta_i} \tag{6}$$

where T is the kinetic energy, V denotes the potential energy, R *is* the Rayleigh's dissipation function, and F is the external force for each dynamic component of the system by assuming that there is no friction and gravitational effect on the control system. The kinetic potential and dissipated energy become when putting Eqs. (1)–(5) into Eqs. (7)–(9), then

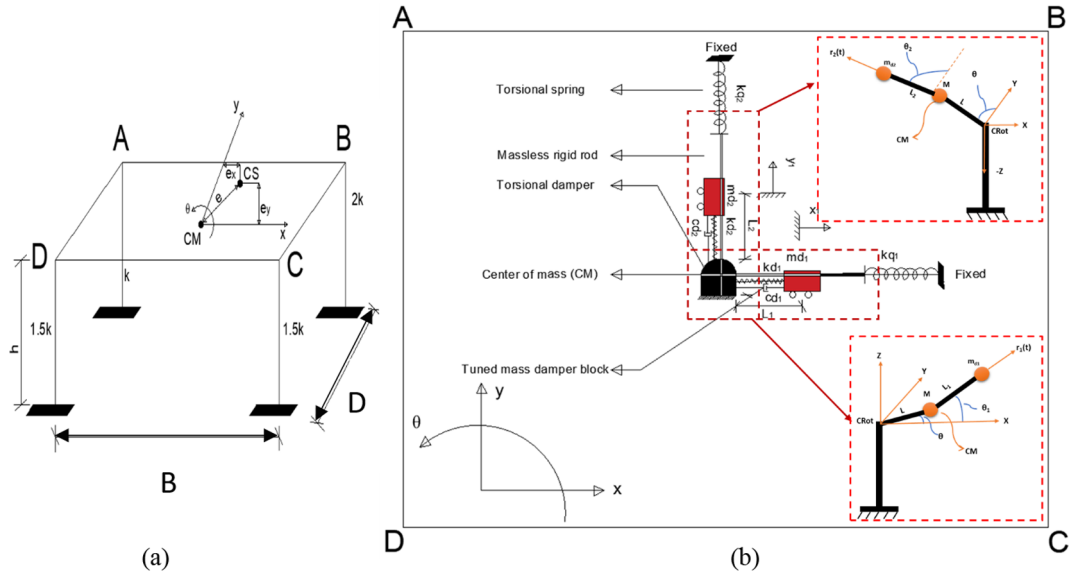

Fig. 3. One story two-way eccentric building: (a) Building 3-D view; (b) control system representation.

The kinetic energy is

$$T = \frac{1}{2}M(\dot{x}_m{}^2 + \dot{y}_m{}^2) + \frac{1}{2}I_m(\dot{\theta}_m)^2 + \frac{1}{2}m_{d1}(\dot{x}_1{}^2 + \dot{y}_1{}^2) + \frac{1}{2}m_{d2}(\dot{x}_2{}^2 + \dot{y}_2{}^2) \tag{7}$$

The potential energy is

$$V = \frac{1}{2}K_x x_s{}^2 + \frac{1}{2}K_y y_s{}^2 + \frac{1}{2}K_\theta\theta(t)^2 + \frac{1}{2}k_{d1}[(x_1{}^2 - x^2) + (y_1{}^2 - y^2)] + \frac{1}{2}k_{q1}(\theta_1(t) - \theta(t))^2 + \frac{1}{2}k_{d2}[(x_2{}^2 - x^2) + (y_2{}^2 - y^2)] + \frac{1}{2}k_{q2}(\theta_2(t) - \theta(t))^2 \tag{8}$$

The Rayleigh's dissipation function is

$$R = \frac{1}{2}C_x\dot{x}(t)^2 + \frac{1}{2}C_y\dot{y}(t)^2 + \frac{1}{2}C_\theta\dot{\theta}(t)^2 + \frac{1}{2}c_{d1}((\dot{x}_1 - \dot{x}_m)^2 + (\dot{y}_1 - \dot{y}_m)^2) + \frac{1}{2}c_{q1}(\dot{\theta}_1(t) - \dot{\theta}(t))^2 + \frac{1}{2}c_{d2}((\dot{x}_2 - \dot{x}_m)^2 + (\dot{y}_2 - \dot{y}_m)^2) + \frac{1}{2}c_{q2}(\dot{\theta}_2(t) - \dot{\theta}(t))^2 \tag{9}$$

The equations above can be linearized if the displacements are assumed small so that $cos(\theta_1) and cos(\theta_2) \approx 1$ and $sin(\theta_1) \approx \theta_1$, $sin(\theta_2) \approx \theta_2$. When Taylor series expansion is used to linearize the nonlinear system about the equilibrium position $(x(t), y(t) and \theta(t)=0)$, the constants $k_{d1}e_x$ or $k_{d1}L_1$, etc. become zero. Hence these constants are not taken into account while constructing the matrices. The mass matrix, stiffness, and damping become by governing the Lagrangian equation (Eq. (6)) as follows:

$$M_{st} = \begin{bmatrix} M & 0 & Me_y & . & . & . & 0 \\ 0 & M & -Me_x & . & . & . & . \\ Me_y & -Me_x & I_m & 0 & . & . & . \\ . & . & 0 & m_{d1} & 0 & . & . \\ . & . & . & 0 & I_{d1} & 0 & . \\ . & . & . & . & 0 & m_{d2} & 0 \\ 0 & . & . & . & . & 0 & I_{d2} \end{bmatrix}$$

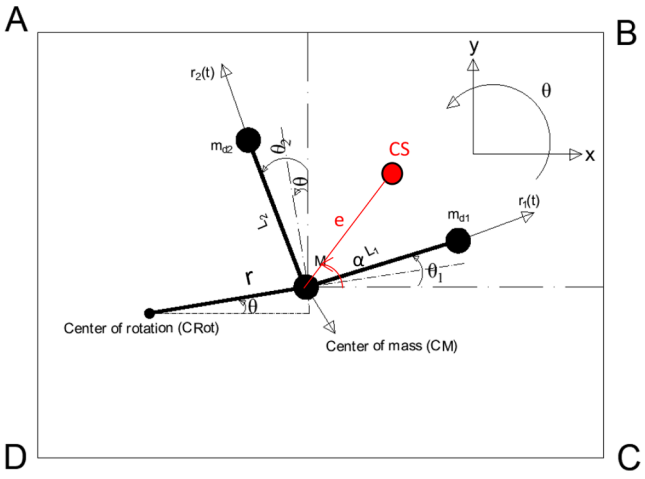

Fig. 4. The simplified equivalent of the structure with the ICS.

inertia and torsional stiffness of the main structure and they are shown in Eqs. (12) and (13).

$$e_x = e.\,cos(\alpha), \quad e_y = e.\,sin(\alpha) \tag{10}$$

$$r_x = \frac{B}{\sqrt{12}}, \quad r_y = \frac{D}{\sqrt{12}}, \quad r = \sqrt{r_x{}^2 + r_y{}^2} \tag{11}$$

$$I_m = M.\,r^2, \quad I_{d1} = m_{d1}(L_1 + r_1)^2, \quad I_{d2} = m_{d2}(L_2 + r_2)^2 \tag{12}$$

$$K_\theta = K_x.\frac{B^2}{2} + K_y.\frac{D^2}{2} \tag{13}$$

$$K_{st} = \begin{bmatrix} K_x + k_{d1} + k_{d2} & 0 & . & -k_{d1} & . & . & k_{d2}(L_2 + r_2) \\ 0 & K_y + k_{d1} + k_{d2} & . & . & -k_{d1}(L_1 + r_1) & -k_{d2} & . \\ . & . & K_\theta + k_{q1} + k_{q2} & 0 & -k_{q1} & . & -k_{q2} \\ -k_{d1} & . & 0 & k_{d1} & k_{d1}e_y & . & . \\ 0 & -k_{d1}(L_1 + r_1) & -k_{q1} & k_{d1}e_y & k_{q1} & 0 & . \\ . & -k_{d2} & . & . & 0 & k_{d2} & -k_{d2}e_x \\ k_{d2}(L_2 + r_2) & . & -k_{q2} & . & . & -k_{d2}e_x & k_{q2} \end{bmatrix}$$

$$C_{st} = \begin{bmatrix} C_x + c_{d1} + c_{d2} & 0 & (c_{d1} + c_{d2})e_y & -c_{d1} & . & . & c_{d2}(L_2 + r_2) \\ 0 & C_y + c_{d1} + c_{d2} & -(c_{d1} + c_{d2})e_x & . & -c_{d1}(L_1 + r_1) & -c_{d2} & . \\ (c_{d1} + c_{d2})e_y & -(c_{d1} + c_{d2})e_x & C_\theta + c_{q1} + c_{q2} + (c_{d1} + c_{d2})e^2 & -c_{d1}e_y & -c_{q1} + c_{d1}e_x(L_1 + r_1) & c_{d2}e_x & -c_{q2} - c_{d2}e_y(L_2 + r_2) \\ -c_{d1} & . & -c_{d1}e_y & c_{d1} & 0 & . & . \\ 0 & -c_{d1}(L_1 + r_1) & -c_{q1} + c_{d1}e_x(L_1 + r_1) & 0 & c_{q1} + c_{d1}(L_1 + r_1)^2 & . & . \\ . & -c_{d2} & c_{d2}e_x & . & . & c_{d2} & . \\ c_{d2}(L_2 + r_2) & . & -c_{q2} - c_{d2}e_y(L_2 + r_2) & . & . & . & c_{q2} + c_{d2}(L_2 + r_2)^2 \end{bmatrix}$$

where M and K_x, K_y are the mass and stiffness of the main structure in the x- and y-translational directions. e_x and e_y are the absolute eccentricity with respect to the CM and r_x and r_y are the radius of gyration of the structure in the x- and y-directions. I_m and K_θ are the polar mass of

Assume that $(L_1 + r_1)$ and $(L_2 + r_2)$ are constants and bounded as:

$$L_1 + r_1(t)^{min} \le (L_1 + r_1) \le L_1 + r_1(t)^{max} \tag{14}$$

$$L_2 + r_2(t)^{min} \le (L_2 + r_2) \le L_2 + r_2(t)^{max} \tag{15}$$

where L_1 and L_2 are the initial length of the linear damper and spring and $r_1(t)$ and $r_2(t)$ are the diagonal response of the ICS under a seismic load.

3.2. State-space representation

The equation of motion, for a two-way eccentric structure, can be mathematically expressed as follows:

$$[M_{st}]\{\ddot{\delta}(t)\} + [C_{st}]\{\dot{\delta}(t)\} + [K_{st}]\{\delta(t)\} = -[M_{st}]\{\Gamma\}\ddot{z}_g \tag{16}$$

$$\{\delta(t)\} = \begin{Bmatrix} x(t) \\ y(t) \\ \theta(t) \\ r_1(t) \\ \theta_1(t) \\ r_2(t) \\ \theta_2(t) \end{Bmatrix}, \{\dot{\delta}(t)\} = \begin{Bmatrix} \dot{x}(t) \\ \dot{y}(t) \\ \dot{\theta}(t) \\ \dot{r}_1(t) \\ \dot{\theta}_1(t) \\ \dot{r}_2(t) \\ \dot{\theta}_2(t) \end{Bmatrix}, \{\ddot{\delta}(t)\} = \begin{Bmatrix} \ddot{x}(t) \\ \ddot{y}(t) \\ \ddot{\theta}(t) \\ \ddot{r}_1(t) \\ \ddot{\theta}_1(t) \\ \ddot{r}_2(t) \\ \ddot{\theta}_2(t) \end{Bmatrix}, \ddot{z}_g = \begin{Bmatrix} \ddot{x}_g \\ \ddot{y}_g \end{Bmatrix}, \text{and} \{\Gamma\} = \begin{bmatrix} 1 & 0 \\ 0 & 1 \\ 0 & 0 \\ 1 & 0 \\ 0 & 0 \\ 0 & 1 \\ 0 & 0 \end{bmatrix}$$

where, M_{st}, C_{st}, and K_{st} are respectively the *nxn* matrix of mass, damping, and stiffness of the structure.$\delta(t)$, $\dot{\delta}(t)$ and $\ddot{\delta}(t)$ are the *n*-dimensional displacement velocity and acceleration vector to the base excitation, $\ddot{x}_g$ and $\ddot{y}_g$ are the input ground motions in the × and y-direction, and Γ is the modification vector of the earthquake excitation. Then the state-space representation of Eq. (16) can be written as:

$$\dot{Z}(t) = AZ(t) + B\ddot{z}_g(t) \tag{17}$$

$$X(t) = C_r Z(t) + D_r \ddot{z}_g(t) \tag{18}$$

$$Z(t) = \begin{bmatrix} \delta(t) \\ \dot{\delta}(t) \end{bmatrix}, A = \begin{vmatrix} zeros(n,\ n) & eye(n,\ n) \\ -M_{st}^{-1}K_{st} & -M_{st}^{-1}C_{st} \end{vmatrix}, B = \begin{bmatrix} zeros(n,\ 2) \\ -\Gamma \end{bmatrix} \tag{19}$$

$$C_r = [eye(n,\ n)\ \ zeros(n,\ n)], \quad D_r = [zeros(n,\ 1)] \tag{20}$$

where *Z (t)* is the (*2nx1*) state vector, *A* is the (*2nx2n*) system matrix, *B* is the (*2nx2*) input matrix, and C_r (*nx2n*) and D_r (*nx2*) are the output matrix and the direct transmission matrix, respectively. They are defined according to the desired output. In this condition, the desired output of state space is the displacements.

4. Design procedure of the ICS

Before applying the proposed ICS to the main structure, the equivalent dynamic properties (M_u, C_u, and K_u) of the main structure for two orthogonal and torsional directions need to be computed. Then the geometric properties (e_x, e_y, and r_x, r_y) of the main structure are carried out. After obtaining the dynamic and geometric characteristics of the main structure, the fundamental frequencies for the first-three dominant-modes are found by solving the eigenvalue problem, see Table 1. Hereafter, the first traditional TMD is placed from CM through x-direction, while the second TMD is implemented in the y-direction. They are tuned to the first-two orthogonal modes and acquired the design parameters (μ_1, L_1, ξ_{d1}, k_{d1}, c_{d1} and μ_2, L_2, ξ_{d2}, k_{d2}, c_{d2}) where they are respectively mass ratio, initial length damping ratio, stiffness and damping constants for the first and second traditional TMDs. Right now, we can compute total length ($L_1 + r_1^{max}$ and $L_2 + r_2^{max}$) of torsional pendulum parts of ICS, which is bounded by the initial length of linear damper/spring and the maximum response of TMDs under selected input earthquake excitations. The ICS is tuned by using generalized Den Hartog equations in the torsional direction and the dynamic properties for torsional spring and damping constants of the first and second TMDs connected (k_{q1}, c_{q1}, and k_{q2}, c_{q2}) are obtained, see Fig. 5. Now, the ICS is ready to be implemented, and its performance was compared with the traditional TMDs in the orthogonal direction which they have the same dynamic properties and mass ratio with the ICS, see Table 1.

4.1. Optimum fundamental properties of the TMDs and the ICS

There are significant optimum parameters to suppress the response of the main structure by using TMD, which are a mass ratio, tuning natural frequency ratio and damping ratio. The first thing is done by selecting the effective mass ratio of the structure and TMD in orthogonal directions as$\mu = \frac{m_{di}}{m} = 5\%$, where m_{d1} and m_{d2} are the mass of TMDs. The mass ratio of the ICS for torsional direction (μ_{qu}) can be governed by using Eq. (21). The structural damping ratio (ξ) is assumed to be 2%, and the frequencies of the structure governed can be computed by Eq. (25). The damping ratio (ξ_{di}) and natural frequency (ω_{di}) of the TMDs are obtained by using generalized Den Hartog equations [39].

$$\mu_{qu} = \frac{I_{d1} + I_{d2}}{\sum I_m} \tag{21}$$

$$\xi_{di} = \sqrt{\frac{3\mu}{8(1+\mu)}} + \frac{0.1616\xi}{1+\mu} \ \ or \ \ \xi_{qi} = \sqrt{\frac{3\mu_{qu}}{8(1+\mu_{qu})}} + \frac{0.1616\xi}{1+\mu_{qu}} \tag{22}$$

$$\omega_i = \sqrt{\frac{K_x}{M_x}}, \ \ \sqrt{\frac{K_y}{M_y}} \ \ or \ \ \sqrt{\frac{K_\theta}{I_m}} \tag{23}$$

$$\omega_{di} = q_i \omega_i \tag{24}$$

where, q_i is the frequency ratio of the TMD and the structure, obtained using:

$$q_i = \frac{1}{1+\mu}(1 - 1.5906\xi)\sqrt{\frac{\mu}{1+\mu}} \tag{25}$$

Then, the stiffness and damping coefficients of the ICS and TMD in torsional and translational directions can be computed by governing Eqs. (26) and (26). It is tabulated, as seen in Table 1.

$$k_{di} = m_{di}\omega_i^2 or k_{qi} = I_{di}\omega_i^2 \tag{26}$$

$$c_{di} = 2\xi_{di}\sqrt{k_{di}m_{di}} \ \ or \ \ c_{qi} = 2\xi_{di}\sqrt{k_{di}m_{di}} \tag{27}$$

Table 1
The first three fundamental frequencies of the main structure and design properties of the TMDs and the ICS.

Main structure	TMD design properties in orthogonal directions					
	L_1	k_{d1}	c_{d1}	L_2	k_{d2}	c_{d2}
w_x (rad/sec)	(m)	(kN/mm)	(kN.s/mm)	(m)	(kN/mm)	(kN.s/mm)
12.87	10	66.67	1.57	10	23.91	0.94
w_y (rad/sec)	ICS design properties in torsional direction					
7.71	$L_1 + r_1^{max}$	k_{q1}	c_{q1}	$L_2 + r_2^{max}$	k_{q2}	c_{q2}
w_θ (rad/sec)	(m)	(kN.mm/rad)	(kN.mm.s/rad)	(m)	(kN.mm/rad)	(kN.mm.s/rad)
20.88	10.18	1.90E + 10	2.02E + 08	10.20	1.91E + 10	2.03E + 08

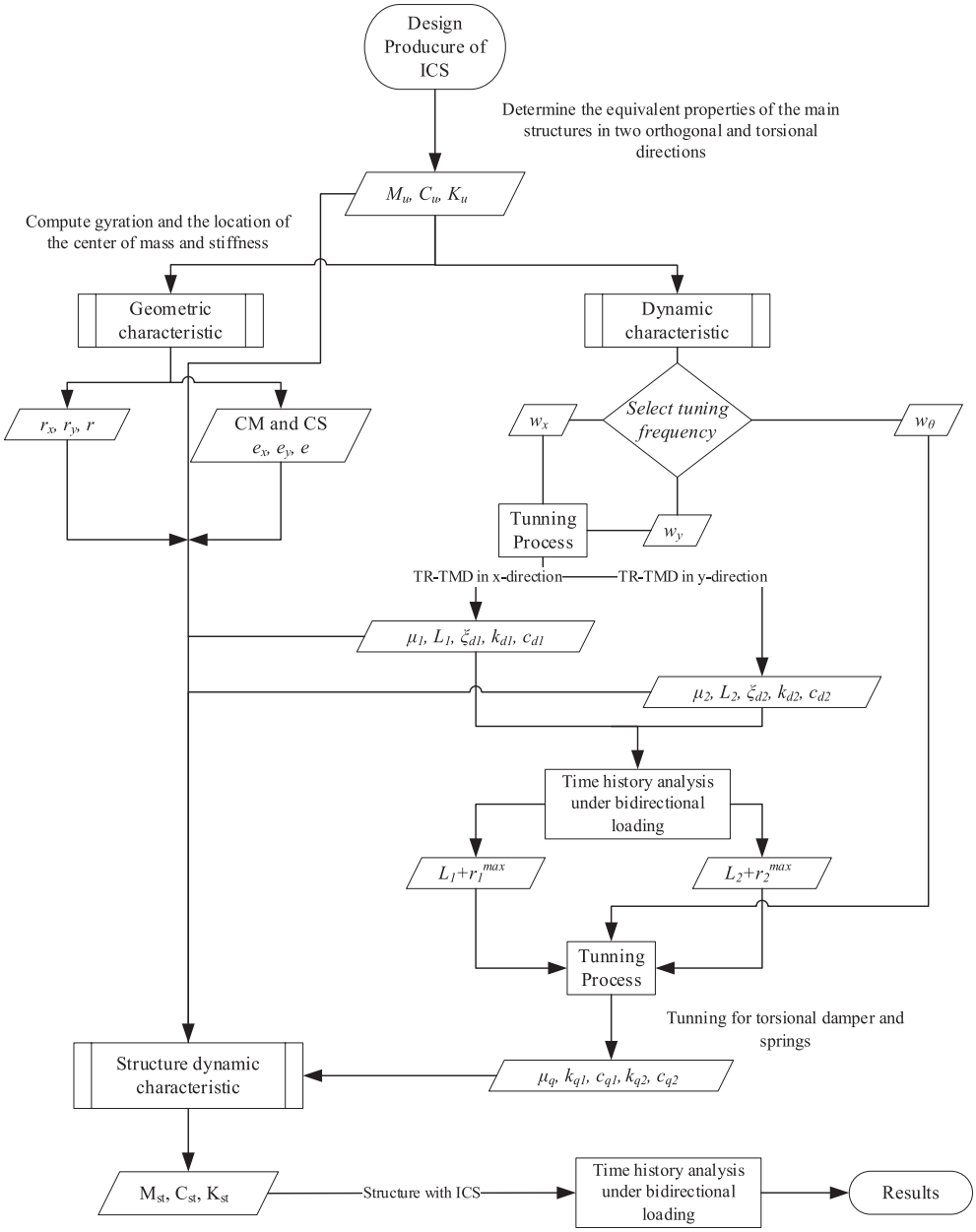

Fig. 5. Structural design and analysis procedure of the structure with the ICS.

5. Model overview

5.1. Description of Benchmark building

In the details of the Benchmark 9-story steel structure, the columns are simply connected to the ground and made of 345 MPa steel. The bays are 9.15 m between the two axes in both horizontal directions with five bays in the x- and y-direction. The columns are wide-flange. Moment resisting frames (MRFs) and simply connected frames (SCFs) are defined as seen in Fig. 6b. The interiors bays of the structures are the simple connection with the composite floor. The floors are composite structures, defined as rigid diaphragms, which provides the relative response to one another for each node under dynamic loading. The floors and bays are comprised of 248 MPa steel acting together at each floor level. The seismic mass of the ground level is 9.65×10^5 kg, for the first level is 1.01×10^6 kg, for the second through eighth levels is 9.89×10^5 kg and for the ninth level is 1.07×10^6 kg. The seismic mass of the above-ground levels of the entire structure is 9.00×10^6 kg. The 9-story N-S MRF is depicted in Fig. 7. For further detailed information about the structural design, the readers are referred to [40].

5.2. The simplified equivalent system of the Benchmark structure

Assuming that the slab for each floor behaves as a rigid diaphragm, all horizontal loads transfer directly to the columns. The response for each node of the floor is relative to one another under an earthquake force. All structures are simplified with two translational (x- and y-) and one rotational (θ-) degree of freedom in each story, see Fig. 7a and b.

Assuming that shear deformation in elements are neglected, and there is a 10% moment reduction at the splices, the lateral stiffness of moment-resisting frames (MRFs) can be computed similarly for any values I_b and I_c using frame stiffness [42], as can be seen in Eqs. (28)

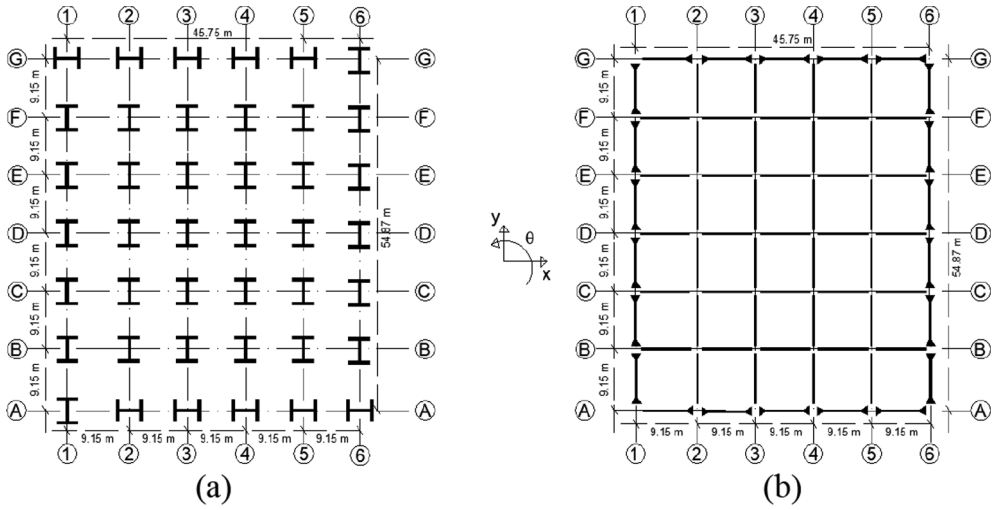

Fig. 6. The 9-story Benchmark buildings modified it from [41]: (a) Plan view and column orientations; (b) connection types of frames.

and (29). For the simple-connected frames, the stiffness contribution is taken into account by governing Eq. (30). Total stiffness for each floor is obtained, as seen in Table 2.

$$k = \frac{24EI_c}{h^3}\frac{12\rho + 1}{12\rho + 4} \tag{28}$$

$$\rho = \frac{I_b}{4I_c} \tag{29}$$

$$k = \frac{3EI_c}{h^3} \tag{30}$$

where$k$ is the equivalent stiffness for a simply connected frame and a moment-resisting frame (MRF), ρ is the beam-to-column stiffness ratio, I_c andI_b are respectively moments of inertia for selected beams and columns, E is the elasticity of the material and h is the height of the floor. The inherent (geometric) eccentricity of the structure for each floor is calculated and taken as Table 2.

5.3. Implementation of the ICS

As stated earlier, a traditional TMD can dissipate energy from only the direction that it is placed and only effective the frequency of the main structure that it is tuned, so its torsional capacity is generally ignored by engineers or negligibly small for torsional response reductions. In this research, the ICS is investigated. The implementation of the proposed ICS, which is operational in both the horizontal directions and the torsional direction, is illustrated in Fig. 6a and traditional TMDs placed in the orthogonal directions are also shown in Fig. 6b. Finally, the ICS is applied to the top floor of Benchmark building to test its performance as compared to the TMDs which have the same dynamic properties with the ICS, see Table 1 above.

5.4. Ground motions

In order to test the influence of the ground motion characteristics on

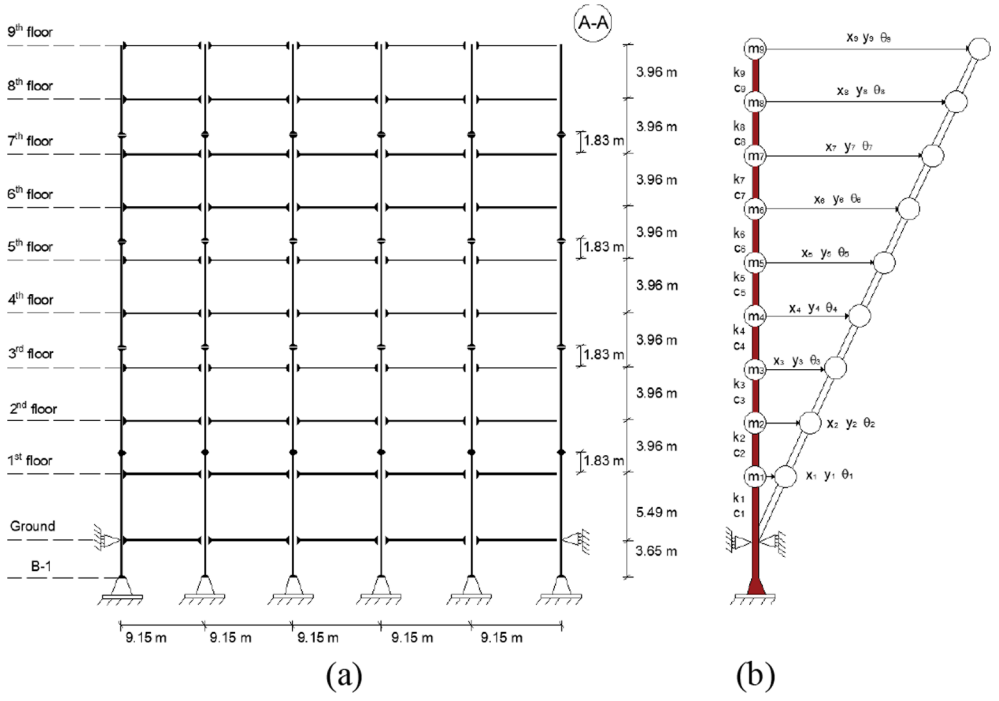

Fig. 7. The nine-story Benchmark building: (a) Elevation-views; (b) simplified equivalent system.

Table 2
The structural components, dynamic and geometric properties of the 9-story benchmark building.

Story no	Structural components				Dynamic properties (stiffness (N/m))		Geometric properties (eccentricity (m))	
	Heights(m)	Exterior Col.	Interior Col.	Beam	x direct.	y direct.	e_x	e_y
1	5.49	W14x370	W14x500	W36x160	7.38E + 09	1.96E + 09	6.63	1.76
2	3.96	W14x370	W14x500	W36x160	7.51E + 09	2.62E + 09	3.53	1.23
3	3.96	W14x370	W14x455	W36x135	6.99E + 09	2.80E + 09	7.67	3.07
4	3.96	W14x370	W14x455	W36x135	6.41E + 09	2.47E + 09	6.18	2.38
5	3.96	W14x283	W14x370	W36x135	5.56E + 09	1.99E + 09	3.32	1.19
6	3.96	W14x283	W14x370	W36x135	5.07E + 09	1.75E + 09	2.16	0.75
7	3.96	W14x257	W14x283	W30x99	3.62E + 09	1.65E + 09	1.75	0.80
8	3.96	W14x257	W14x283	W27x84	3.11E + 09	1.55E + 09	1.58	0.79
9	3.96	W14x233	W14x257	W24x68	2.75E + 09	1.66E + 09	1.21	0.73

Table 3
The selected real-saved earthquakes information.

Earthquake input	Recording station	PGA (Peak Ground Acceleration)		Dominant direction
		N-S comp. (m/s^2)	W-E comp. (m/s^2)	
El Centro	Imperial Valley Irrigation District in 1940	3.417	2.101	N-S (x)
Loma Prieta	Oakland Outer Harbor Wharf Channel 1 and Channel 3 in 1989	2.155	2.704	Nearly Both
Kocaeli	The general director of the meteorology of Duzce District in 1999	2.197	3.543	W-E (y)

the proposed control system, in this study, some of the most devastating and strong real-life earthquake data were acquired from the database [43]. The dynamic responses of the system were evaluated under N-S and W-E components of the real earthquake excitations of El Centro in 1940 from the station of Imperial Valley Irrigation District, Loma Prieta in 1989 from the station of Channel 1 and Channel 3 and Kocaeli earthquake in 1999 from the station of the general director of meteorology of Duzce District, see Table 3. The accelerations versus time data are illustrated in Fig. 9.

6. Performance evaluation criteria and seismic energy analysis

Spencer et al. [44] proposed and established a set of fifteen performance criteria (PC) for the Benchmark building for comparison of performance evaluation (PE) of various control systems. The smaller values of one of these PC are more desirable for improved effectiveness. For performance evaluation in this study, energy analyses and three performance criteria are selected the maximum; floor displacement (J_1), drift (J_2), and floor acceleration (J_3).

$$J_1\left\{\begin{matrix}ElCentro\\LomaPrieta\\Kocaeli\end{matrix}\right\} = max\left\{\frac{max\ |\delta_i(t)|}{\delta^{max}}\right\} \tag{31}$$

$$J_2\left\{\begin{matrix}ElCentro\\LomaPrieta\\Kocaeli\end{matrix}\right\} = max\left\{\frac{max\ |d_i(t)|/h_i}{d_n{}^{max}}\right\} \tag{32}$$

$$J_3\left\{\begin{matrix}ElCentro\\LomaPrieta\\Kocaeli\end{matrix}\right\} = max\left\{\frac{max\ |\ddot{\delta}_i(t)|}{\ddot{\delta}^{max}}\right\}\ for\ \ i = 1\ \ to\ \ n \tag{33}$$

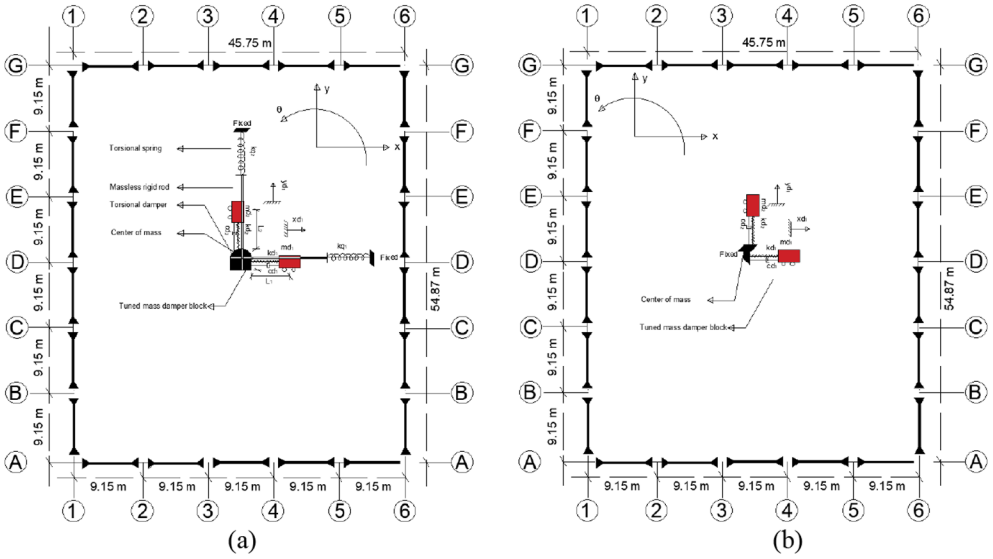

Fig. 8. A schematic representation of; (a) the ICS and (b) TMDs at the top floor of the Benchmark building.

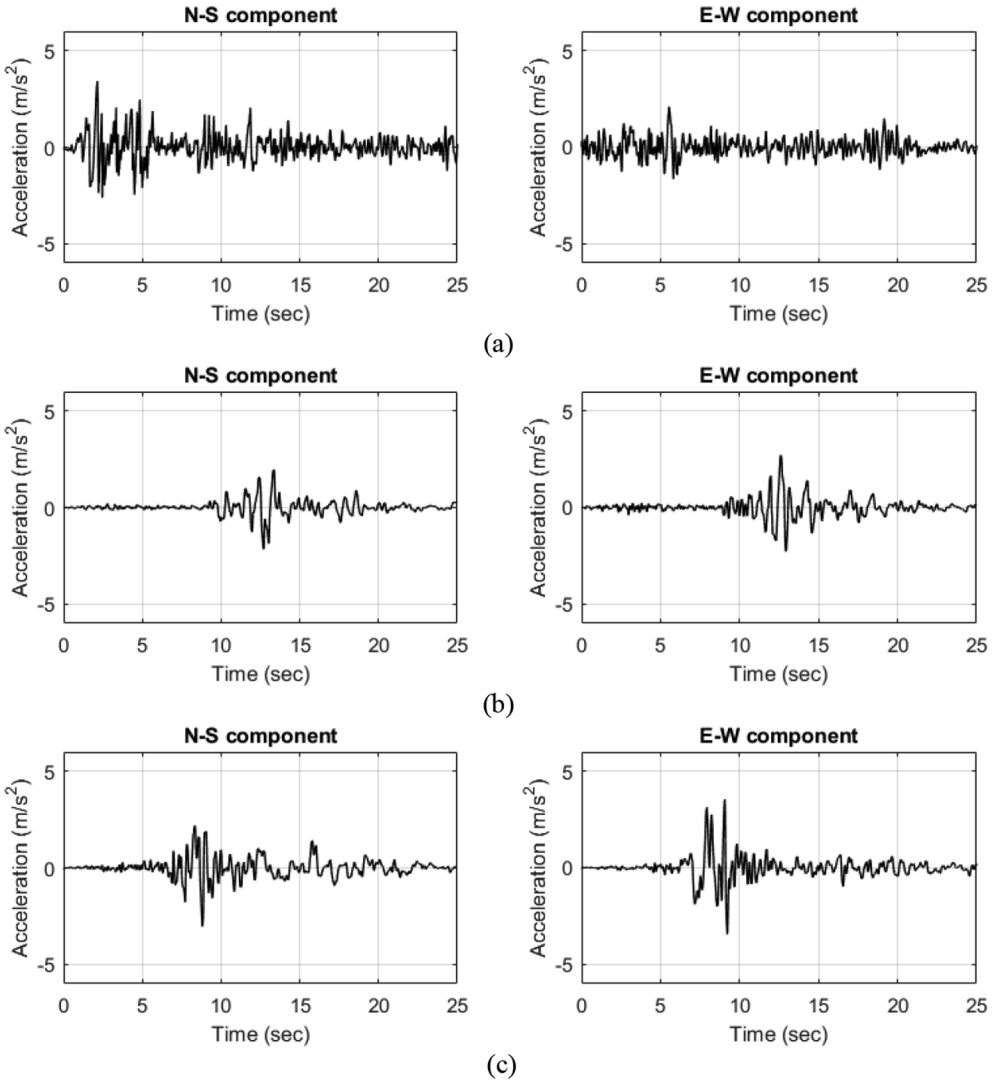

Fig. 9. The N-S and E-W components of the saved real-life earthquake data: (a) El Centro; (b) Loma Prieta; (c) Kocaeli earthquake.

where, $|\delta_i(t)|$ is the absolute displacement of the controlled system at the ith floor. δ^{max} is the maximum absolute displacement of the uncontrolled system at any floor. $|d_i(t)|$ is the inter-story drift of the floor above ground level. h_i is the height of the ith floor. The ${d_n}^{max}$ is the maximum absolute inter-story ratio at any floor (${d_n}^{max} = max\{d_i(t)\}/h_i$)). $|\ddot{\delta}_i(t)|$ is the absolute displacement of the controlled system at the ith floor. $\ddot{\delta}^{max}$ is the maximum absolute acceleration of the uncontrolled system at any floor.

The general equation of motion for an MDOF system can be expressed in terms of energy computation as follow [45];

$$\int_0^t \dot{\delta}^T(\tau)[M_{st}]\ddot{\delta}(\tau)d\tau + \int_0^t \dot{\delta}^T(\tau)[C_{st}]\dot{\delta}(\tau)d\tau + \int_0^t \dot{\delta}^T(\tau)[K_{st}]\delta(\tau) = -\int_0^t \dot{\delta}^T(\tau)[M_{st}]\vec{\Gamma}\ddot{z}_g(\tau)d\tau \quad (34)$$

The energy equations can be written as;

$$E_{kr} + E_d + E_a = E_{ir} \quad (35)$$

In which E_{ir} stands for the relative input energy, E_{kr} is the relative kinetic energy, E_d is the damping energy, and E_a is the strain energy, as formulated below;

$$E_{kr} = \frac{1}{2}\dot{\delta}^T(\tau)[M_{st}]\dot{\delta}^T(\tau) \quad (36)$$

$$E_d = \int_0^t \dot{\delta}^T(\tau)[C_{st}]\dot{\delta}(\tau)d\tau \quad (37)$$

$$E_a = \int_0^t \dot{\delta}^T(\tau)[K_{st}]\delta(\tau) \quad (38)$$

Table 4
The first five modal frequencies of the structures.

Modal frequency (rad/s)	Benchmark building	Benchmark building with TMDs	Benchmark building with ICS	Dominant direction	Modal effective mass (tonne)
1st mode	7.706	6.369	6.574	y lateral	7515.8
2nd mode	12.868	8.736	9.032	x lateral	7142.1
3rd mode	20.88	10.515	10.592	y lateral	1004
4th mode	26.185	14.707	14.792	θ torsional	14.7
5th mode	33.248	21.012	18.858	x lateral	1090.6

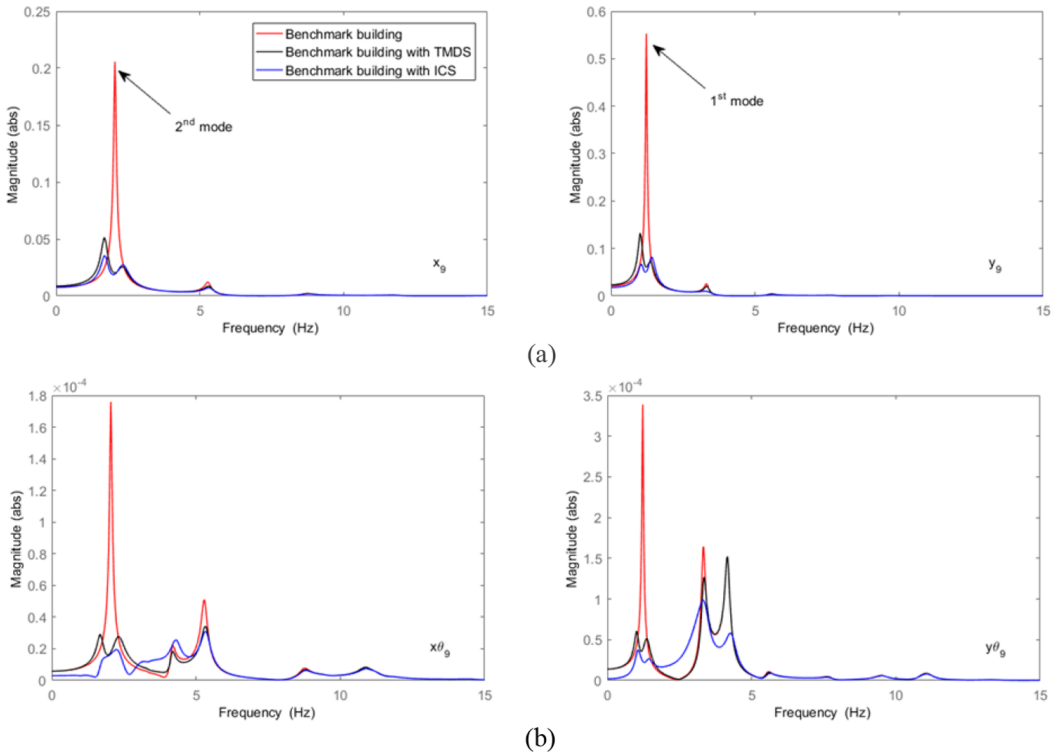

Fig. 10. Top floor displacement transfer functions for the Benchmark building and its application with the TMDs and the ICS: (a) x_9 and y_9 translational transfer functions; (b) $x\theta_9$ and $y\theta_9$ coupling transfer functions.

$$E_{ir} = -\int_0^t \dot{\delta}^T(\tau)[M_{st}]\vec{\Gamma}\ddot{z}_g(\tau)d\tau \tag{39}$$

7. Simulation results and discussion

The SAC Benchmark 9-story steel structure was picked, and the analyses were conducted on the Benchmark building by retrofitting it with the two Tuned Mass Dampers (TMDs) in two orthogonal directions and Integrated Control System (ICS) as shown in Fig. 8. In order to test the performance of the proposed ICS under the bidirectional loading case, the two TMDs -which have the same dynamic properties with ICS- were placed in two orthogonal directions. The dynamic analysis results for the Benchmark building and its respective application with the TMDs and the ICS were obtained and compared with each other.

While tuning TMDs to the first two translational directions (7.706 rad/s and 12.868 rad/s), the ICS were tuned to the first two translational and rotational directions to the fundamental frequency (7.706 rad/s, 12.868 rad/s, and 20.880 rad/s) of the Benchmark building. The calculated dynamic properties and the first five model frequencies of the model structures are respectively tabulated in Table 1 and Table 4.

The frequency responses (transfer functions), which are independent of the characteristics of the earthquake inputs, were selected to test the effectiveness of the proposed ICS in the seismic response control of the structures. The amplitudes of the top floor x- and y-translational and rotational (coupling due to eccentricity) frequency responses, respectively, are shown in Fig. 10a and b.

It is observed that the second mode dominates the x-response when the building is subjected to x-directional ground excitation, while the first mode controls y-response when it is subjected to y-directional ground excitation, see Fig. 10a. Therefore, the ICS and TMDs were designed to control the 2nd vibration mode of the Benchmark building for the first TMD, placed in the x-direction and control the 1st vibration mode for the second TMD, applied in the y-direction. The properties of the ICS and TMDs computed from Eq. (17) through Eq. (23) are shown in Table 1.

Table 5
The peak and RMS displacement response of the Benchmark building with or without TMDs and ICS.

Earthquake input	Type of structures	Displacements on the top floor					
		Peak resp. (cm) or (10^{-3}rad)			RMS resp. (cm) or (10^{-3}rad)		
		x	y	θ	x	y	θ
El Centro	Benchmark building	8.25	10.66	0.117	2.05	3.12	0.032
	Benchmark building with the TMDs	6.52	7.56	0.090	1.28	1.42	0.021
	Benchmark building with the ICS	5.16	6.11	0.064	1.05	1.14	0.016
Loma Prieta	Benchmark building	4.39	17.10	0.143	1.03	5.32	0.035
	Benchmark building with the TMDs	4.07	13.04	0.115	0.74	2.08	0.017
	Benchmark building with the ICS	3.47	12.47	0.091	0.60	2.04	0.013
Kocaeli	Benchmark building	6.29	13.18	0.194	1.61	4.08	0.033
	Benchmark building with the TMDs	6.12	12.20	0.159	1.01	2.79	0.021
	Benchmark building with the ICS	5.25	10.43	0.143	0.84	1.92	0.018

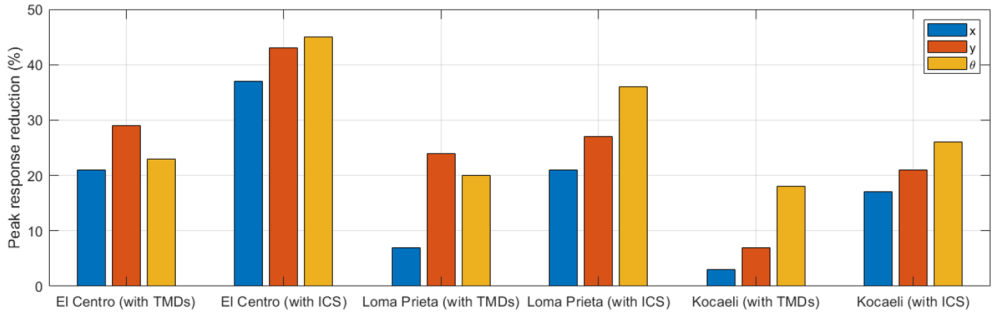

(a)

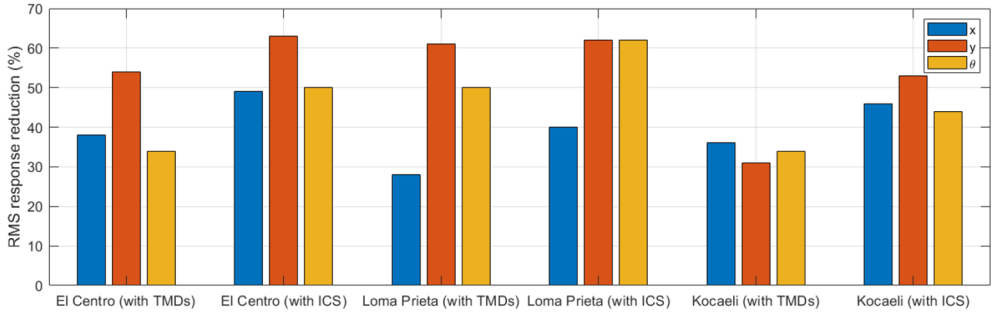

(b)

Fig. 11. The percentage of the response reduction: (a) for the peak responses; (b) for RMS responses.

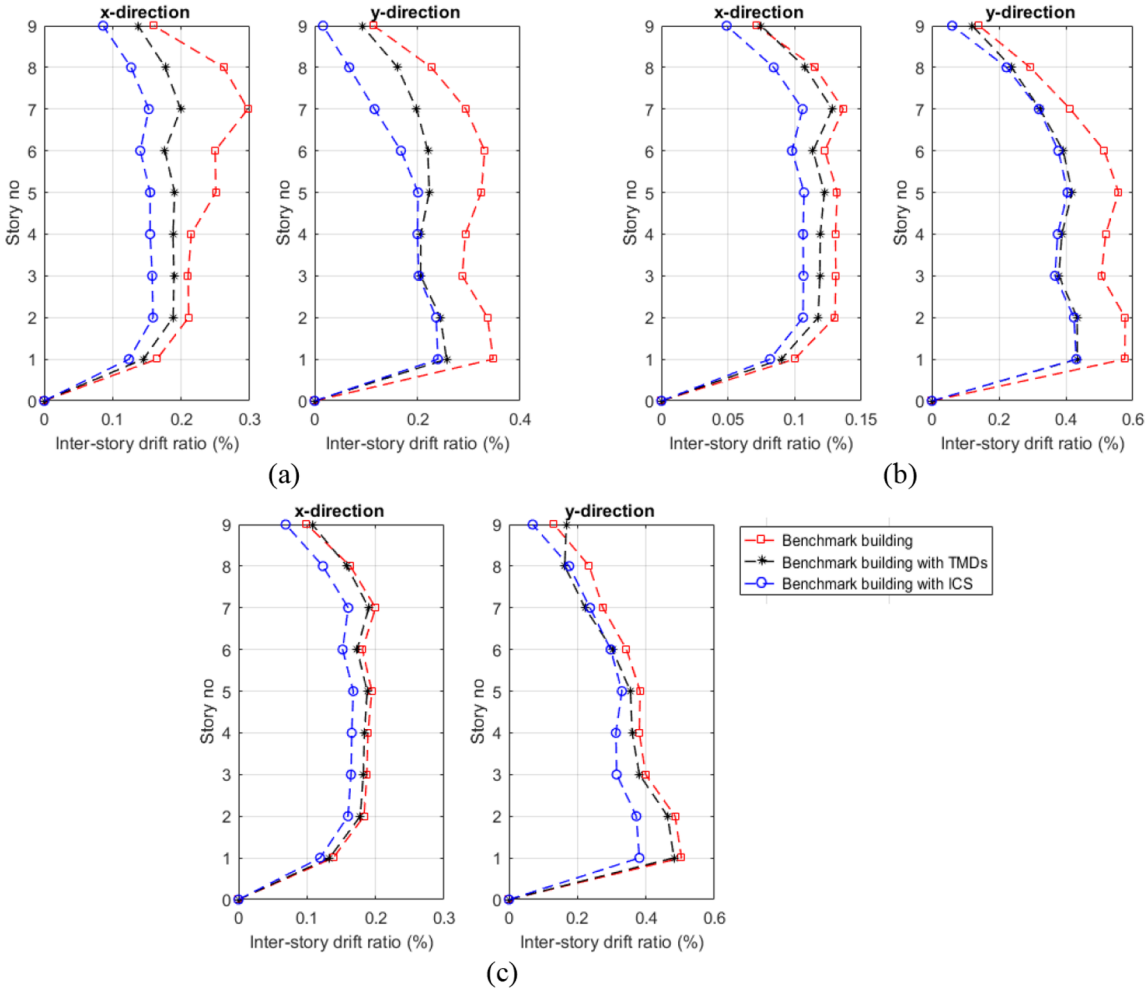

Fig. 12. Maximum inter-story drift ratio of the structures when subjected to bidirectional ground excitations: (a) El Centro; (b) Loma Prieta; (c) Kocaeli earthquake.

As seen in Fig. 10, the amplitude of the frequency response of the Benchmark building with the ICS are substantially reduced not only in translational directions, but also especially in rotational (coupling) directions compared to the cases where the Benchmark building is only equipped with the individual TMDs. Thus, the effectiveness of the proposed ICS for simultaneously reducing the x- and y-translational and the rotational seismic responses of the elastic two-way eccentric building was validated.

To perform response history analyses for the structure with the TMDs and the ICS, the analytical models need to be accurately constructed and coded in the structural analytical program package. Therefore, the time history simulations were performed in Matlab & Simulink [46], and the results were obtained and saved for evaluation purpose.

As expected from the results presented in Table 5 that the bare Benchmark building experiences the highest peak amplitude for x- and y-translational and θ-rotational direction at the top floor when respectively subjected to bidirectional El Centro, Loma Prieta and Kocaeli bidirectional ground motions. The table also shows the comparison of the peak and the Root Mean Square (RMS) results, which is used to measure the intensity of vibration, to evaluate accumulative structural response for each of the structures. Overall, the performance of the ICS for response reductions in three directions is substantially improved as compared to the performance of the orthogonal TMDs.

It indicates the peak and RMS response reduction in x-, y- and θ-directions for the building with the TMDs and the ICS comparing the bare Benchmark building under the real saved bidirectional ground motions which are El Centro, Loma Prieta, and Kocaeli earthquake. It is seen from Fig. 11a and 11b, the ICS has significantly suppressed the magnitude of the peak and RMS displacements in the three directions simultaneously as compared to the TMDs.

The inter-story drift ratio is a useful response quantity for structural (earthquake) engineers and an indicator of structural performance, especially for high-rise buildings. The inter-story drift ratios in the x- and y-directions can be reduced overall of structures by strengthening the Benchmark building respectively with TMDs and ICS for El Centro, Loma Prieta, and Kocaeli earthquake. It is important to note that the ICS successfully improves the inter-story drift ratios performance in the translational directions as compared to the TMDs, see Fig. 12.

In developing an energy-based design approach and assessing the damage potential of structures, it is useful to learn the distribution of earthquake input energy among other energy components: kinetic (E_{kr}),

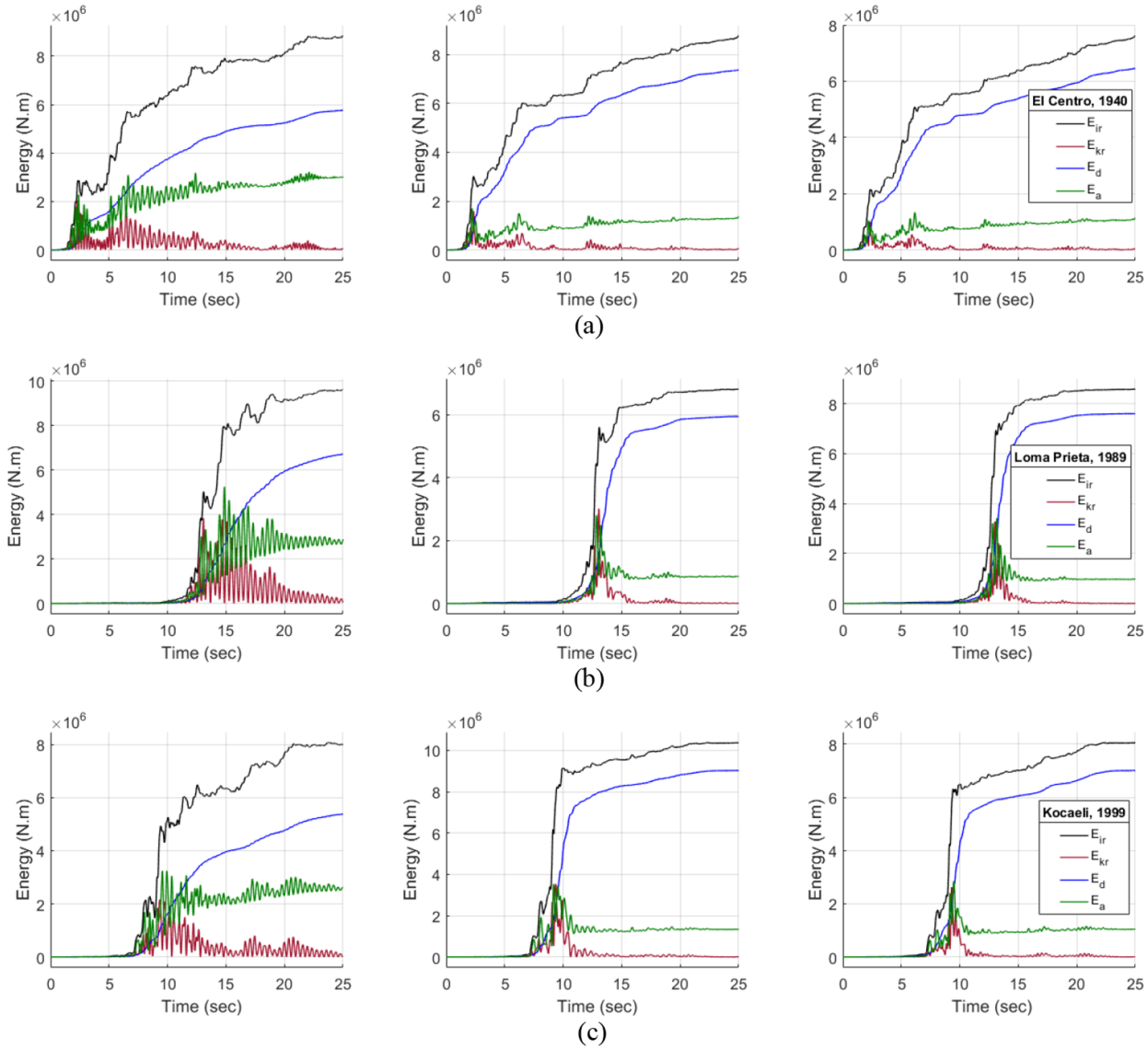

Fig. 13. The total energy of the model structures, which are the bare Benchmark building, Benchmark building with TMD and Benchmark building with ICS respectively when subjected to bidirectional ground excitations: (a) El Centro; (b) Loma Prieta; (c) Kocaeli earthquake.

Table 6
The total energy of the structures.

Earthquake input	Type of structures	Total energy			
		Kinetic energy	Damping energy	Strain energy	Input energy
		(E_{kr})(kN.m)	(E_d)(kN.m)	(E_a)(kN.m)	(E_{ir})(kN.m)
El Centro	Benchmark building	38	5760	3042	8840
	Benchmark building with TMDs	32	7360	1370	8762
	Benchmark building with ICS	22	6459	1141	7622
Loma Prieta	Benchmark building	35	6723	2882	9640
	Benchmark building with TMDs	6.5	5952	854.5	6813
	Benchmark building with ICS	2.5	7600	972.5	8575
Kocaeli	Benchmark building	5.4	5377	2618	8000.4
	Benchmark building with TMDs	6.4	9024	1337	10367.4
	Benchmark building with ICS	2.9	7009	1041	8052.9

elastic strain (E_a), and damping (E_d) [47]. The energy components of the Benchmark building and its corresponding application with the TMDs and the ICS are, therefore, respectively illustrated in Fig. 13a–c for bidirectional earthquake excitation of El Centro, Loma Prieta, and Kocaeli. The energy components are also tabulated in Table 6.

The input energy (E_{ir}) to a structure is a critical measure for structural performance during an earthquake, and it depends proportional to the relationship between relative velocity and the ground acceleration [48]. The Benchmark building has the maximum input energy with 8840 kN.m as well as it's kinetic energy is the maximum with 38 kN.m, because it undergoes the fastest relative velocity among the others under bidirectional El Centro earthquake excitations. For the Loma Prieta earthquake, the Benchmark building still has the maximum input energy with 9640 kN.m. However, the input energy of the structure with the ICS (8575 kN.m) is larger than with TMDs (6813 kN.m). This is because the structure with the ICS has relatively bigger relative velocity as compared to the model with TMDs. Furthermore, under the bidirectional excitations of Kocaeli earthquake, while the maximum input energy (10367.4 kN.m) belongs to the structure with TMDs, the Benchmark building has the minimum energy (8000.4 kN.m), see Table 6. This is because the earthquake input is dominant in the y-translational direction, and this can cause detuning effects for the Loma Prieta and Kocaeli earthquake bidirectional loading case. That is why, instead of decreasing relative velocity comparing to the Benchmark building, it increases.

It is a well-known fact that the earthquake is arbitrary and unpredictable shaking of the ground, so the Benchmark building and its respective application with TMDs and ICS might be exposed to x-dominant or y- dominant or both or θ-dominant excitations. In addition to this fact, the effectiveness of TMDs is dependent upon the characteristics of the input ground motions. Therefore, the tuning design was made and kept it the same for any loading cases for the first and the second TMD. The first was placed in the x-direction, which is controlled by 2nd mode and the second is applied in the y-direction controlled by 1st mode of the Benchmark structure. This design assumption might lead the control systems to experience detuning effects in case of the dominant direction of the bidirectional loading case, as seen in Loma Prieta and Kocaeli earthquake.

The strain energy is another indicator to test structural performance, and it has a strong relationship to the structural damages. The bearing systems of a structure; columns and beams have capacities that can dissipate energy safely. If those capacities are exceeded, structural damages could be the outcome under earthquakes. There are gradually decreased in the overall strain by implementing, in acceding order, of the Benchmark building, the TMD and the ICS on the building under El Centro and Kocaeli earthquakes, except Loma Prieta, see Table 6. This is because the relative velocity is more dominant to determine the strain energy quantity than the relative displacement under the Loma Prieta earthquake. In conclusion, using the TMDs and the ICS as a control system on the Benchmark building increases the strain energy reduction as compared to the bare structure even in the detuning case like Loma Prieta and Kocaeli earthquakes.

Table 7 shows overall performance evaluation for the control systems; TMDs and ICS by comparing to the bare Benchmark building. The notations (J_1, J_2, and J_3) represent performance evaluation, in order, peak drift ratio, peak acceleration, and peak base shear. There is a substantial reduction for both the tuning case (El Centro earthquake) and the detuning case (Loma Prieta and Kocaeli earthquakes). For both tuning and detuning loading case, the values of the peak responses (J_1-J_3), are less than one for most of the cases, except that the peak base shear in y-direction under Kocaeli earthquake is slightly higher than the uncontrolled case. Thus, for this earthquake, the Benchmark building

Table 7
Performance evaluation of the model structures.

Earthquake input	Type of structures	Performance evaluation					
		J_1		J_2		J_3	
		x-direc.	y-direc.	x-direc.	y-direc.	x-direc.	y-direc.
El Centro	Benchmark building	–	–	–	–	–	–
	Benchmark building with TMD	0.811	0.711	0.671	0.739	0.701	0.761
	Benchmark building with ICS	0.659	0.623	0.535	0.691	0.668	0.746
Loma Prieta	Benchmark building	–	–	–	–	–	–
	Benchmark building with TMD	0.918	0.757	0.932	0.753	0.681	0.901
	Benchmark building with ICS	0.803	0.735	0.786	0.747	0.652	0.929
Kocaeli	Benchmark building	–	–	–	–	–	–
	Benchmark building with TMD	0.968	0.932	0.949	0.956	0.972	1.033
	Benchmark building with ICS	0.851	0.794	0.838	0.756	0.970	0.931

controlled by orthogonal TMDs in x- and y-direction are not protected as effective as by the ICS. All values with detuning effects are slightly less or greater than the uncontrolled structure. Under detuning circumstances, overall, the ICS performs better than the TMDs.

8. Conclusion

The purpose of this paper was to examine and investigate the performance of the proposed Integrated Control System (ICS) when subjected to selected bidirectional ground motions which lead either to tuning effects or to detuning effects. Additionally, the Benchmark building is controlled by two traditional Tuned Mass Dampers (TMDs), which are respectively applied in the x- and y-direction, for verifying the effectiveness of the ICS. The following conclusions were pointed out from the numerical results:

1. There is a substantial reduction of the frequency response validated the effectiveness of the ICS in controlling the seismic responses for two-way eccentric elastic buildings.
2. Unlike traditional TMDs placed in two orthogonal directions, the ICS is more comprehended to control not only two orthogonal (x- and y-) directions, but also effectively control rotational (θ-) direction. By means of the proposed system configuration, the structures first-three dominants modes can effectively be controlled by the ICS regardless of any external energy sources.
3. The tuning design of the ICS is flexible since it depends on design parameters such as the initial lengths, the linear/torsional dampers, and springs coefficients, the mass ratio, and the location of the ICS. The ICS is, therefore, highly capable of enhancing the control capacity of the structure conveniently in multi-directions. With the help of the flexible design of ICS, the torsional response is substantially reduced.
4. The ICS is also more robust in restricting the inter-story drift ratio as compared with TMDs. It sufficiently mitigates the RMS and peak displacement on the top floor of the Benchmark building. Thus, the ICS has a better performance than the TMDs in terms of response reductions.
5. The strain energy (E_a) has a strong relationship with the damage level of the structural components. Despite the detuning effect of the proposed ICS for two-way eccentric buildings, the results show that it can significantly reduce the strain energy demands. Thus, the ICS is also effective in reducing the potential seismic damage to two-way asymmetric-plan buildings under bidirectional ground excitations.
6. According to the performance evaluation criteria, there are substantial reductions for both the tuning case (El Centro) and the detuning case (Loma Prieta and Kocaeli earthquakes). For both cases, the performance indexes are overall less than the bare Benchmark building and its respective application with the TMDs. Therefore, the effectiveness of ICS performance is verified.

Declaration of Competing Interest

The authors declare that they have no known competing financial interests or personal relationships that could have appeared to influence the work reported in this paper.

Acknowledgment

The authors would like to thankfully acknowledge the Ministry of National Education of the Republic of Turkey for providing the opportunity and scholarship during the first author's doctoral study in the United States of America. This research did not receive any specific grant from funding agencies in the public, commercial, or not-for-profit sectors.

References

[1] Ross AS, El Damatty AA, El Ansary AM. Application of tuned liquid dampers in controlling the torsional vibration of high rise buildings. Wind Struct An Int J 2015;21:537–64. https://doi.org/10.12989/was.2015.21.5.537.
[2] FEMA 750. NEHRP (National Earthquake Hazards Reduction Program) Recommended Seismic Provisions for New Buildings and Other Structures (FEMA P-750), 2009 Edition. 2009.
[3] Raheem SEA, Ahmed MMM. Abdel-shafy MMAAGA. Evaluation of plan configuration irregularity effects on seismic response demands of L-shaped MRF buildings. Bull Earthq Eng 2018;16:3845–69. https://doi.org/10.1007/s10518-018-0319-7.
[4] Özhendekci N, Polat Z. Torsional irregularity of buildings. In: 14th World Conf. Earthq. Eng., 2008.
[5] Özmen G, Girgin K, Durgun Y. Torsional irregularity in multi-story structures. Int J Adv Struct Eng 2014;6:121–31. https://doi.org/10.1007/s40091-014-0070-5.
[6] Akyürek O, Suksawang N, Go TH, Tekeli H. Performance evaluation of a reinforced concrete building strengthened respectively by the infill wall, active and passive tuned mass damper under seismic load. Comput Struct 2019;223:106097. https://doi.org/10.1016/j.compstruc.2019.07.006.
[7] Akyürek O. Lateral and Torsional Seismic Vibration Control for Torsionally Irregular Buildings. Florida Institute of Technology; 2019.
[8] Akyürek O, Tekeli H, Demir F. Plandaki dolgu duvar yerleşiminin bina performansı Üzerindeki Etkisi (the effects of infill walls located in plan on buildings performance). Int J Eng Res Dev 2018;30:42–55. https://doi.org/10.29137/umagd.419660.
[9] Erduran Emrah, Ryan KL. Effects of torsion on the behavior of peripheral steel-braced frame systems. Earthq Eng Struct Dyn 2010;40:491–507. https://doi.org/10.1002/eqe.
[10] Damjan M, Fajfar P. On the inelastic seismic response of asymmetric buildings under bi-axial excitation. Earthq Eng Struct Dyn 2005;34:943–63. https://doi.org/10.1002/eqe.463.
[11] Chen C-H, Lai J-W, Mahin SA. Seismic performance assessment of concentrically braced frames. In: 13 World Conf Earthq Eng 2004:1–8. http://doi.org/10.1061/(ASCE)ST.1943-541X.0002276.
[12] Akyürek O. Betonarme Bina Performansina Dolgu Duvarlarin Etkisi (The effects of infill walls in RC building performance). Suleyman Demirel Univertsity; 2014.
[13] Hartog JPDEN. Mechanical Vibrations; 1985.
[14] Li C. Performance of multiple tuned mass dampers for attenuating undesirable oscillations of structures under the ground acceleration. Earthq Eng Struct Dyn 2000;29:1405–21. https://doi.org/10.1002/1096-9845(200009)29:9<1405::AID-EQE976>3.0.CO;2-4.
[15] Xu K, Igusa T. Dynamic characteristics of multiple substructures with closely spaced frequencies. Earthq Eng Struct Dyn 1992;21:1059–70. https://doi.org/10.1002/eqe.4290211203.
[16] Igusa T, Xu K. Vibration control using multiple tuned mass dampers. J Sound Vib 1994;175:491–503. https://doi.org/10.1006/jsvi.1994.1341.
[17] Yamaguchi H, Harnpornchai N. Fundamental characteristics of Multiple Tuned Mass Dampers for suppressing harmonically forced oscillations. Earthq Eng Struct Dyn 1993;22:51–62. https://doi.org/10.1002/eqe.4290220105.
[18] Jangid RS. Dynamic characteristics of structures with multiple tuned mass dampers. Struct Eng Mech 1995;3:497–509. https://doi.org/10.12989/sem.1995.3.5.497.
[19] Park J, Reed D. Analysis of uniformly and linearly distributed mass dampers under harmonic and earthquake excitation. Eng Struct 2001;23:802–14. https://doi.org/10.1016/S0141-0296(00)00095-X.
[20] Sadek F, Mohraz B, Taylor AW, Chung RM. A method of estimating the parameters of tuned mass dampers for seismic applications. Earthq Eng Struct Dyn 1997;26:617–35. https://doi.org/10.1002/(SICI)1096-9845(199706)26:6<617::AID-EQE664>3.0.CO;2-Z.
[21] Lavan O. Multi-objective optimal design of tuned mass dampers. Struct Control Heal Monit 2017;24:e2008. https://doi.org/10.1002/stc.2008.
[22] Shetty KK, Krishnamoorthy. Multiple Tuned Mass Dampers for Response Control of Multi-Storey Space Frame Structure. J Seismol Earthq Eng 2011; 13: 167–78.
[23] Gill D, Elias S, Steinbrecher A, Schröder C, Matsagar V. Robustness of multi-mode control using tuned mass dampers for seismically excited structures. Bull Earthq Eng 2017;15:5579–603. https://doi.org/10.1007/s10518-017-0187-6.
[24] De Angelis F, Cancellara D. Dynamic analysis and vulnerability reduction of asymmetric structures: fixed base vs base isolated system. Compos Struct 2019;219:203–20. https://doi.org/10.1016/j.compstruct.2019.03.059.
[25] Cancellara D, De Angelis F. Nonlinear dynamic analysis for multi-storey RC structures with hybrid base isolation systems in presence of bi-directional ground motions. Compos Struct 2016;154:464–92. https://doi.org/10.1016/j.compstruct.2016.07.030.
[26] Cancellara D, De Angelis F. A base isolation system for structures subject to extreme seismic events characterized by anomalous values of intensity and frequency content. Compos Struct 2016;157:285–302. https://doi.org/10.1016/j.compstruct.2016.09.002.
[27] Huo L, Li H. Torsionally coupled response control of structures using. In: 13th World Conf. Earthq. Eng.; 2017.
[28] Cancellara D, De Angelis F. Dynamic assessment of base isolation systems for irregular in plan structures : Response spectrum analysis vs nonlinear analysis. Compos Struct 2019;215:98–115. https://doi.org/10.1016/j.compstruct.2019.02.013.
[29] Singh MP, Singh S, Moreschi LM. Tuned mass dampers for response control of torsional buildings. Earthq Eng Struct Dyn 2002;31:749–69. https://doi.org/10.1002/eqe.119.
[30] Ueng JM, Lin CC, Wang JF. Practical design issues of tuned mass dampers for torsionally coupled buildings under earthquake loadings. Struct Des Tall Spec Build 2008;17:133–65. https://doi.org/10.1002/tal.336.
[31] Desu NB, Deb SK, Dutta A. Coupled tuned mass dampers for control of coupled vibrations in asymmetric buildings. Struct Control Heal Monit 2006;13:897–916.

https://doi.org/10.1002/stc.64.
[32] Ahlawat AS, Ramaswamy A. Multiobjective optimal FLC driven hybrid mass damper system for torsionally coupled, seismically excited structures. Earthq Eng Struct Dyn 2002;31:2121–39. https://doi.org/10.1002/eqe.209.
[33] Li C, Qu W. Optimum properties of multiple tuned mass dampers for reduction of translational and torsional response of structures subject to ground acceleration. Eng Struct 2006;28:472–94. https://doi.org/10.1016/j.engstruct.2005.09.003.
[34] Lin CC, Ueng JM, Huang TC. Seismic response reduction of irregular buildings using passive tuned mass dampers. Eng Struct 2000;22:513–24. https://doi.org/10.1016/S0141-0296(98)00054-6.
[35] Tse KT, Kwok KCS, Hitchcock PA, Samali B, Huang MF. Vibration control of a wind-excited benchmark tall building with complex lateral-torsional modes of vibration. Adv Struct Eng 2007;10:283–304. https://doi.org/10.1260/136943307781422208.
[36] Rahman MS, Hassan MK, Chang S, Kim D. Adaptive multiple tuned mass dampers based on modal parameters for earthquake response reduction in multi-story buildings. Adv Struct Eng 2017;20:1375–89. https://doi.org/10.1177/1369433216678863.
[37] Lin JL, Tsai KC, Yu YJ. Bi-directional coupled tuned mass dampers for the seismic response control of two-way asymmetric-plan buildings. Earthq Eng Struct Dyn 2011;40:675–90. https://doi.org/10.1002/eqe.1054.
[38] He H, Wang W, Xu H. Multidimensional Seismic Control by Tuned Mass Damper with Poles and Torsional Pendulums. Shock Vib 2017;2017:1–14. https://doi.org/10.1155/2017/5834760.
[39] Abubakar IM, Farid BJM. Seismic Control Systems: Design and Performance Assessment vol. 2012. Bostan: WITPRES; 2012.
[40] Ohtori Y, Christenson RE, Spencer BF, Dyke SJ. Benchmark control problems for seismically excited nonlinear buildings. J Eng Mech 2004;130:366–85. https://doi.org/10.1061/(ASCE)0733-9399(2004) 130:4(366).
[41] Federal Emergency Management Agency (FEMA). FEMA 355F - State of the Art Report on Performance Prediction and Evaluation of Steel Moment-Frame Buildings. Fema-355F 2000;1:1–367.
[42] Chopra AK. Dynamics of structures: theory and applications to earthquake engineering. vol. 23. Englewood Cliffs, N.J. : Prentice Hall; 2000. http://doi.org/10.1193/1.1586188.
[43] CEE 221: Structural Analysis II n.d. http://www.eng.ucy.ac.cy/petros/Earthquakes/earthquakes.htm (accessed October 9, 2018).
[44] Spencer Jr. BF, Christenson RE, Dyke SJ. Next generation benchmark control problem for seismically excited buildings. In: Second World Conf. Struct. Control, 1998, p. 1135–360.
[45] Wong KKF, Yang R. Earthquake response and energy evaluation of inelastic structures. J Eng Mech 2002;128:308–17. https://doi.org/10.1061/(ASCE)0733-9399(2002) 128:3(308).
[46] MathWorks, M. A. T. L. A. B. SIMULINK for technical computing. Available on https://www.mathworks.com/ 2016.
[47] Khashaee P, Mohraz B, Sadek F, Lew HS, Gross JL. Distribution of Earthquake Input Energy in Structures. Gaithersburg, MD 20899: 2003.
[48] Takewaki I. Bound of earthquake input energy. J Struct Eng 2004;130:1289–97. https://doi.org/10.1061/ASCE0733-94452004130:91289.